

Twisted and coiled bamboo artificial muscles for moisture responsive torsional and tensile actuation

Xiaoyu Hu(胡晓宇), Xueqi Leng(冷雪琪), Tianjiao Jia(贾天娇), Zunfeng Liu(刘遵峰)

Citation: Chin. Phys. B . 2020, 29(11): 118103 . **doi:** 10.1088/1674-1056/abbbda
Journal homepage: http://cpb.iphy.ac.cn; http://iopscience.iop.org/cpb

What follows is a list of articles you may be interested in

Moisture-sensitive torsional cotton artificial muscle and textile

Yuanyuan Li(李媛媛), Xueqi Leng(冷雪琪), Jinkun Sun(孙进坤), Xiang Zhou(周湘), Wei Wu(兀伟), Hong Chen(陈洪), Zunfeng Liu(刘遵峰)

Chin. Phys. B . 2020, 29(4): 048103 . **doi:** 10.1088/1674-1056/ab7745

Tri-band transparent cross-polarization converters using a chiral metasurface

Shi Hong-Yu, Li Jian-Xing, Zhang An-Xue, Wang Jia-Fu, Xu Zhuo

Chin. Phys. B . 2014, 23(11): 118101 . **doi:** 10.1088/1674-1056/23/11/118101

Depth-dependent mosaic tilt and twist in GaN epilayer：An approximate evaluation

Zhang Jin-Feng, Nie Yu-Hu, Zhou Yong-Bo, Tian Kun, Ha Wei, Xiao Ming, Zhang Jin-Cheng, Hao Yue

Chin. Phys. B . 2014, 23(6): 068102 . **doi:** 10.1088/1674-1056/23/6/068102

Twisted and coiled bamboo artificial muscles for moisture responsive torsional and tensile actuation*

Xiaoyu Hu(胡晓宇), Xueqi Leng(冷雪琪), Tianjiao Jia(贾天娇), and Zunfeng Liu(刘遵峰)†

State Key Laboratory of Medicinal Chemical Biology, College of Pharmacy and Chemistry, Key Laboratory of Functional Polymer Materials, Nankai University, Tianjin 300350, China

(Received 28 August 2020; revised manuscript received 10 September 2020; accepted manuscript online 28 September 2020)

Smart textiles responding to the ambient environment like temperature, humidity, and light are highly desirable to improve the comfortability and realize multifunctions. The bamboo yarn has merits like air permeability, biodegradability, and excellent heat dissipation performance, but it has not been prepared for responsive materials and smart textiles. In this paper, the moisture-responsive twisted bamboo yarns were plied to form a self-balanced torsional actuator and wrapped around a mandrel to form a coil, followed by water immersion and evaporation to fix the shape and serve as a tensile actuator. A torsional actuation of 64.4°·mm^{-1} was realized for the twisted actuator in 4.2 s; a maximum elongation of 133% or contraction of 50% was achieved for a coiled tensile actuator with good cyclability. The porous structure of bamboo yarns helped improve the water absorbance speed and decrease the response time of moisture. The self-balanced two-ply physical structure and reversible generation of chemical phase after soaking in aqueous solution fixed internal stress and provided good cyclability. With the unique properties including aqueous water-induced shape fixation and moisture-induced actuation, the application of tensile actuation of bamboo yarns was demonstrated, showing promising prospects on smart textiles.

Keywords: smart textile, bamboo yarn, moisture-responsive, twist

PACS: 81.05.Lg, 87.15.kr, 89.20.Bb, 64.70.km **DOI:** 10.1088/1674-1056/abbbda

1. Introduction

As an important part of smart materials, the smart textiles are getting wider market prospects, and their abundant functions can be realized by integration with flexible electronic units, such as biomedical sensing,[1] energy devices,[2,3] wireless communication,[4] and electromagnetic interference shielding.[5] Some smart textiles can change their characteristics depending on the surroundings such as camouflage[6] or heating.[7] Besides, the smart textiles should have some merits needed for an excellent textile such as air permeability,[8] heat preservation,[9] durability during use,[10] and biocompatibility.[11]

There have been numerous kinds of materials and structures applied in the field of smart textiles, and the natural yarn materials are getting extensive attention because the textile made by synthetic yarns can hardly be degraded and produce a large amount of solid waste.[12] Based on the components, natural yarns are mainly composed of two categories of materials: cellulose and protein. The protein-based natural yarns, such as silk and spider silk, showed outstanding actuation performance metrics and mechanical properties.[13,14] However, the cellulose-based natural yarns including cotton,[15] flax,[16] and bamboo[17] are much cheaper and have easier availability than protein-based yarns. The hydroxyl groups in the cellulose species provide adequate sites for hydrogen bonding with water molecules, resulting in remarkable hygroscopicity and comfortability of the textiles. Bamboo yarns have some unique advantages among the cellulose-based natural yarns for the reasons below. First, the air permeability and the capability of heat dissipation of the bamboo yarns are extraordinary because of the high porosity and interconnected holes.[18] Secondly, the unique antibacterial property of the bamboo yarns makes it a safe and promising candidate for smart textiles.[19] Thus the bamboo yarns can be an important alternative to satisfy featured requirements and diverse sources of the textile industry.

Except for the material selection, the unique structures of the yarns can give newly-developed applications for the smart textiles. The twist-based actuators with twist, self-coil, or mandrel coil structure can generate large actuation strokes and work capacity by volume expansion upon exposure to small molecules like water and organic solvents.[20,21] In our previous work, the self-balanced structure was applied on the silk textiles to expand and shrink the pore size in an ambient environment with respective low and high humidity, which greatly increased the comfortability.[22] The moisture-responsive torsional actuation of cotton yarns was also used for the intelligent window.[15] It is still of significance to realize smart cloth-

*Project supported by the State Key Development Program for Basic Research of China (Grant Nos. 2016YFA0200200 and 2017YFB0307001), the National Natural Science Foundation of China (Grant Nos. 51973093, U1533122, and 51773094), and the Natural Science Foundation of Tianjin, China (Grant No. 18JCZDJC36800).

†Corresponding author. E-mail: liuzunfeng@nankai.edu.cn

© 2020 Chinese Physical Society and IOP Publishing Ltd

ing in a wider range of materials, especially for bamboo yarns with superior air permeability, heat dissipation, and antibacterial property. Furthermore, besides structural designs in the geometrical level (*e.g.* coiling and plied structure), the new shape fixation and actuation mechanism in the microstructural level need to be exploited in the area of moisture-responsive smart textiles.

In this work, the plied and moisture-activated torsional actuator made by porous bamboo yarns was first demonstrated, showing a peak torsional stroke of $64^\circ \cdot mm^{-1}$ in an actuation period of 4.2 s. The abundant pores in the meso- and macroscale were responsible for the high water absorption speed. The contraction or elongation motion was realized by mandrel coiling and shape fixation by soaking in water and drying. The unique properties of water-immersion-induced shape fixation and moisture-induced actuation were first found in bamboo yarns rather than previously reported water-responsive natural yarns. The application of bamboo yarns for smart textiles was demonstrated by the tensile actuation of mandrel-coiled units.

2. Experimental section

The bamboo yarn thread (73 dtex) was purchased from Nantong Yiheng New Material Technology Co., Ltd., which was composed of multiple plies of monofilaments. After the preparation of the muscles below, they were exposed in water fog or environment with specified humidity for a relatively short time (< 10 s) to actuate.

2.1. Fabrication of self-balanced torsional bamboo artificial muscles

First, one end of the bamboo yarn was fixed on the rotational axis of a 42-step servomotor (Model 42BYGH40-1704A, Huatian Technology Co., Ltd.), while the other end was torsionally tethered to prevent untwist during the following step and loaded with a weight to generate stress (called twisted stress). After isobaric twist insertion to a certain degree, the loading during twist was slowly moved to the midpoint of the twisted yarn while its two ends were still torsionally tethered. After the formation of the plied structure, the torsional tethering can be removed. If the actuation stress was different from the twisted stress, another weight can be used with two ends of the muscle torsionally tethered.

2.2. Fabrication of plied bamboo artificial muscles for elongation and contraction

The fabrication of artificial muscles providing tensile actuation was similar to the procedures described above. After twist insertion and formation of plies, the self-balanced torsional muscle yarn was wrapped around a mandrel. When the chirality of the torsional muscle and the mandrel coiling was the same (*ZZ*), it was called plied homochiral muscle to give contraction during actuation. When the chirality of the above two was opposite (*ZS*), the muscles were aimed to elongate upon actuation and called plied heterochiral muscle. For the heterochiral muscles, the adjacent coils should contact with each other to obtain a large elongation. For the homochiral muscles, the neighboring coils should be wrapped with a certain distance, which was called unit coil pitch, to give space for muscle contraction. The muscle was immersed in water at room temperature for 0.5 h to fix the shape.

2.3. Characterizations

The pore sizes and porosity were measured and analyzed by an adsorption analyzer (ASAP 2460). The degassing temperature was set at 150 °C to remove water molecules when getting away from decomposition. The x-ray diffraction (XRD) was performed on a Rigaku Smart Lab system equipped with a 3.0-kW generator (Japan). The wavelength of x-ray was 1.54 Å by using Cu-$K\alpha$ source radiation and the 2θ scanning rate was $5^\circ \cdot min^{-1}$. SEM images were obtained on a scanning electron microscope (model MERLIN Compact, ZEISS). The cross-sectional image was obtained by cutting the sample in liquid nitrogen. The mechanical properties of the muscles were measured by using a mechanical tester (Shanghai Heng Wing Precision Instrument Co., Ltd., Model: HY-0580) with a stretching rate of 5 $mm \cdot min^{-1}$. The humidity was set at 30% for the mechanical test. A hygrometer (CEMDT-615) was used for recording ambient temperature and humidity.

2.4. Fitting methods of XRD curves

The crystalline component and the content of the bamboo fibers were calculated by the multi-peak fitting of the XRD curve and areal calculation of the corresponding peaks, using Cu-$K\alpha$ radiation diffraction angles ranging from 5° to 30°. The details of peak fitting are as follows. The peak fitting was conducted using Peakfit software. The amorphous peak ends should overlap the measured XRD curve and the positions can vary during fitting. The peak center positions for the crystalline phases were obtained directly from the recorded XRD curve and only the shape and width of these peaks can adjust during fitting. Pearson VII functions were used for fitting curves. The contents of phases were calculated based on the area ratio of corresponding peaks to the total area of the measured curves.

3. Results and discussion

3.1. Structure and mechanical properties of the bamboo yarn

The natural bamboo yarn is mainly composed of polysaccharides such as cellulose, hemicellulose, and lignin, all of which have abundant hydroxyl groups.[17] For a better understanding of the bamboo yarn, the cross-sectional SEM images were taken and illustrated as shown in Fig. 1(a). The bamboo yarns with a diameter of ~ 230 μm were assembled by multiple monofilaments. The SEM image with increase magnification showed that the bamboo monofilament was porous. The SEM images of the yarn surface shown in Fig. 1(b) again proved that the yarn was composed of multiple parallel-aligned monofilaments before twist insertion. After twist insertion with twist density of 900 turns/m, the direction of the yarn was also biased, with the bias angle to the yarn axis (α) measured as $\sim 32.3°$. Equation (1) was shown below to calculate α based on the twist density (T) and yarn diameter (d) for a twisted, non-coiled yarn[23]

$$\alpha = \tan^{-1}(\pi d T). \tag{1}$$

The calculated bias angle α was 33.0°, which was in accordance with the measured value of 32.3°. The morphology of the two-plied bamboo yarn was shown at the bottom of Fig. 1(b). The direction of spontaneously formed plying of the twisted yarn (S) was opposite to the twist direction (Z). Thus, the two-ply structure balanced some torque to avoid twist release of the twisted yarn and was able to store the torque without torsional tethering, which was favorable for simplifying the structure of yarn-shaped artificial muscles.

The mechanical properties are essential for artificial muscles. Thus, the stress–strain curves of twisted bamboo yarns were tested and illustrated in Fig. 1(c). In addition, the elongation at break and fracturing stress were shown in Fig. 1(d) for comparison. With twist density increasing from 100 turns·m^{-1} to 800 turns·m^{-1}, the elongation at break monotonically decreased from 46.56% to 27.24%, and the breaking stress decreased from 35.06 MPa to 30.69 MPa. However, little change in Young's modulus and stress before fracture were observed. The moderate breaking strength of twisted yarns was a prerequisite for the good performance of artificial muscles.

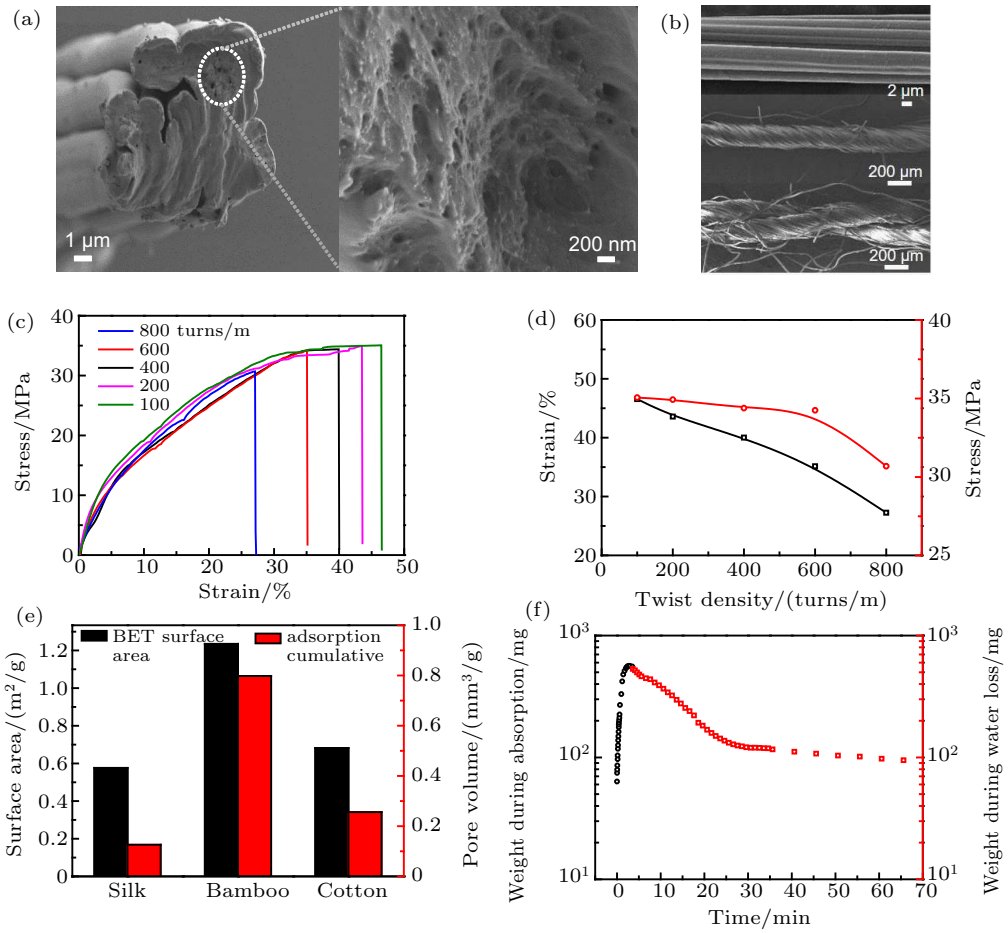


Fig. 1. Structure and mechanical properties for bamboo yarns. (a) SEM images with low (left) and high (right) magnifications showing the cross-sectional monofilaments and porous structure in the micron- and nanometer scale. (b) SEM images of the pristine monofilament (upper), twisted yarn (middle), and two-plied bamboo yarn (lower). (c) Tensile stress–strain curves of bamboo yarns with different twist densities. The elongation rate was 25%·min^{-1}. (d) Elongation at break and fracture strength as a function of twist density for non-plied bamboo yarns. (e) Mesopores of silk, bamboo, and cotton yarns, with surface area calculated by the BET method and pore volume calculated by the adsorption curve of N_2 gas. (f) Kinetics of water absorption and desorption of the bamboo yarn.

The mesoporous structure was measured by an adsorption analyzer, with the effective detection range of pore sizes roughly from 2 nm–50 nm. The bamboo yarns had the largest pore surface area of 1.24 $m^2 \cdot g^{-1}$, larger than that of silk (0.58 $m^2 \cdot g^{-1}$) or cotton yarns (0.68 $m^2 \cdot g^{-1}$) (see Fig. 1(e)). The volume of mesopores for bamboo yarns was 0.798 $mm^3 \cdot g^{-1}$, also higher than values of silk or cotton. It should be noted that pores with larger sizes were also found in bamboo yarns as shown in Fig. 1(a). Thus, the internal porous structure of bamboo monofilaments was observed. To find out possible connections between the porous structure and the moisture actuation, the water absorption curve of bamboo fibers was illustrated as shown in Fig. 1(f). Bamboo fibers with a weight of 63 mg at 20% ambient moisture can absorb water molecules with 7.9 times of its weight in a short period of 3.5 min, obtaining a high water uptake speed of 3.76%·s^{-1}, which was higher than that of the calculated value of the cotton yarn (0.66%·s^{-1})[15] or silk fibers (2%·s^{-1}).[22] The highly porous structure may elongate the water desorption process but for a highly sensitive material responding to moisture, the necessary water uptake might be decreased and thermal heating can be an alternative option to accelerate water evaporation.

3.2. Twisted and plied bamboo yarns for self-balanced torsional artificial muscles

It is reasonable to assume that the bamboo yarn may absorb water because of the polysaccharide-based component and the porous structure. Therefore, we fabricate a kind of moisture-driven artificial muscle that can rotate upon actuation. The schematic illustration for the fabrication of this plied-type torsional muscle was shown in Fig. 2(a), with detailed preparation described in Subsection 2.1. It should be noted that after the formation of the two-plied structure, both ends were torsionally free of tethering during the actuation process. The water molecules in the fog were absorbed by the bamboo yarns, as confirmed by the fact that the diameter of the yarn increased by 15%, with negligible change in the length direction. As illustrated in Fig. 2(b), the volume expansion of the bamboo yarns caused untwisting of the muscle, with a peak torsional stroke of 64.4°·mm^{-1} when the water flow was 0.16 g·s^{-1}·m^{-2}. It is hypothesized that the water molecules may be absorbed in between the gaps in the two plied yarns, among the monofilaments in one twisted yarn and the pores of the monofilament. Thus, after removal of water fog, the water molecules would be released stepwise, causing a fast rotation actuation in 4.2 s followed by a relatively slow reversal process to completely rotate back. The rotation period was about 4.3 min and 5 cycles of torsional stroke were recorded, demonstrating similar actuation behavior.

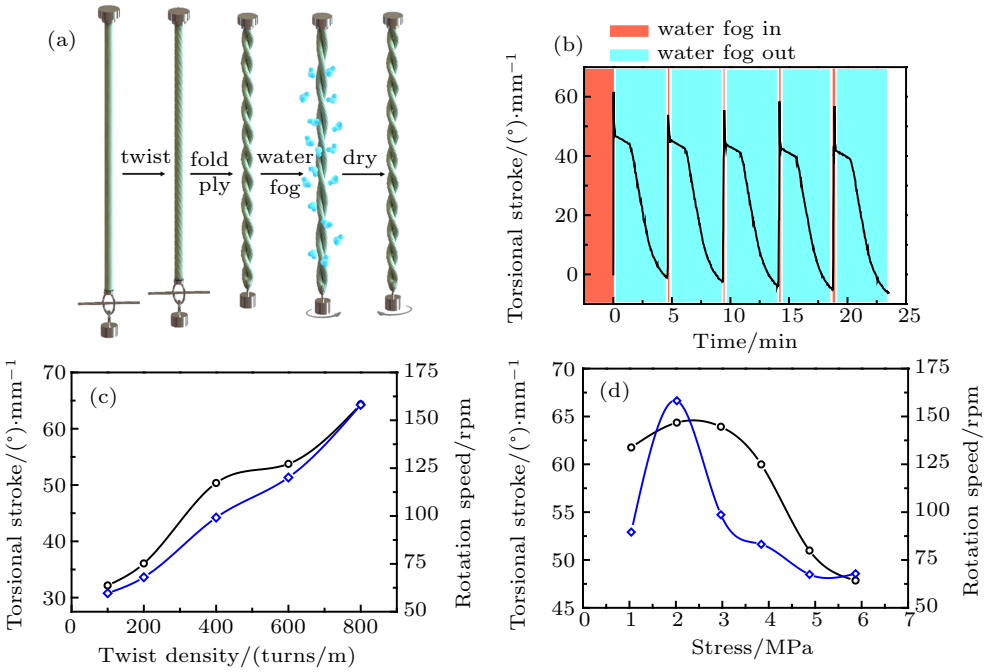


Fig. 2. Fabrication and actuation performance of self-balanced two-ply torsional bamboo muscles. (a) Schematic illustrations of the fabrication of two-ply torsional bamboo muscles. (b) The torsional stroke as a function of time during the first 5 cycles. (c) The torsional stroke and rotation speed as a function of inserted twist. (d) The effect of actuation stress on the torsional actuation performance. For panels (b) and (c), the actuation stress was 2.01 MPa, and for panels (b) and (d), the twist density was 800 turns·m^{-1}.

Furthermore, the relationship between the torsional stroke and the inserted twist was studied (Fig. 2(c)). There was a positive correlation relationship between the twist density with actuation strokes or the rotation speed. The high value of 64.4°·mm^{-1} and 158 rpm was obtained when the twist density reached the highest number of 800 turns·m^{-1}. The effect of actuation stress on the torsional stroke and rotation speed was a little complex as shown in Fig. 2(d). When the actuation

stress was low (< 2.0 MPa), the internal stress might be too low for actuation. However, the torsional stroke as well as the rotation speed decreased with the actuation stress larger than 2.0 MPa. The peak torsional stroke and rotation speed were respectively 67.0°·mm^{-1} and 158.3 rpm at actuation stress of 2.0 MPa.

3.3. Self-balanced, mandrel coiled twisted yarns for tensile actuation

3.3.1. Tensile actuation performance metrics

The yarns in daily life such as cotton yarns and silk were composed of several plies of monofilaments. The above hierarchical structures in the textile industry inspired us to use the yarns with a self-balanced structure as a unit to construct other types of actuators. The fabrication process was illustrated in Fig. 3(a). The two-ply torsional artificial muscle units, which were prepared using the above methods, were subsequently wrapped on a mandrel and fixed by immersing in water, followed by drying in the air for 24 h to fix the coiled shape. After shape fixing, the coiled artificial muscles were obtained and can change their length upon moisture. Elongation was observed when the direction of twist in the plied muscles (Z) and the mandrel coiling (S) was opposite as shown in the results of Fig. 3(b). Thus, both elongation and contraction can be realized by mandrel-coiling, showing good cyclability in the investigated 20 actuation cycles. Increasing the relative humidity or twist density contributed to increasing tensile strokes for both *ZZ* and *ZS* tensile artificial muscles (Fig. 3(c)). For example, with a twist density of 700 turns·m^{-1} and relative humidity increasing from 50% to 90%, the elongation of *ZS*-type muscle increased from 25.9% to 84.7%. The highest elongation was 133% when the muscle with 900 turns/m inserted twist and spring index of 4.3 was actuated at 90% relative humidity. The contractile strain for the *ZZ*-type muscle was usually smaller than the elongation strain of *ZS* muscle when the parameters were the same because more spacing hindrance was encountered during contraction as compared with elongation.

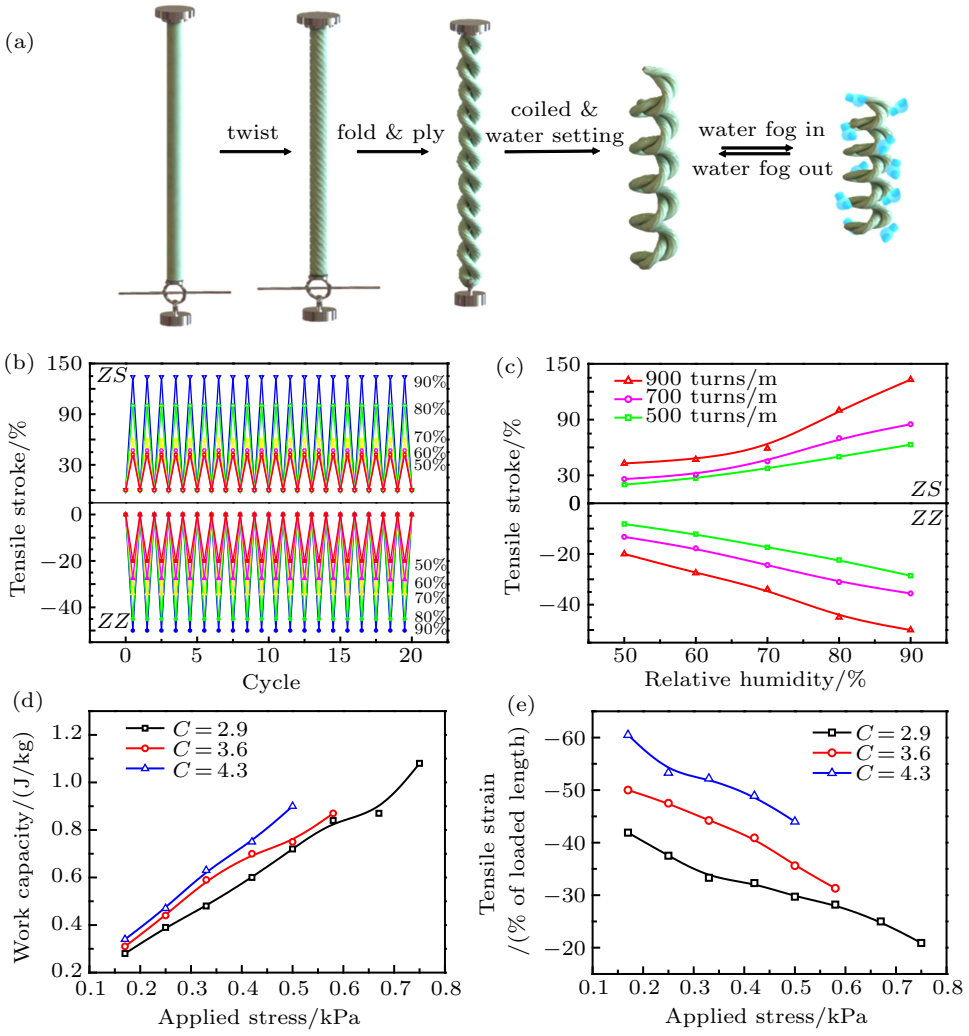


Fig. 3. Fabrication and actuation performances of mandrel coiled bamboo muscles for tensile actuation. (a) Schematic illustrations for the preparation of the tensile muscles. (b) The tensile stroke as a function of the number of actuation cycles for *ZZ*- and *ZS*-type muscles. (c) The tensile stroke for muscles with different twist densities and actuated at various humidities. (d) Work capacity as a function of applied stress for muscles with varied spring index. (e) Tensile strain normalized by loaded length for *ZZ*-type muscles. If not otherwise specified, the twist density was 900 turns·m^{-1}, the spring index was 4.3, the relative humidity was 90%, and the applied stress was 0.33 kPa for panels (b)–(e).

As an important parameter for evaluating artificial muscles or actuators, the work capacity with varied actuation stress was measured for the *ZZ*-type bamboo artificial muscles (Fig. 3(d)). The work capacity (W) was defined as the mechanical work of per mass of artificial muscles and calculated by Eq. (2).

$$W = \frac{Mg\Delta H}{m}. \tag{2}$$

Here, M, ΔH, and m represent the mass of the loading, the rising height during actuation, and the corresponding mass of the muscles. The spring index (C) referred to the ratio of the mandrel diameter to the yarn diameter. It is observed that W monotonically increased with the applied actuation stress in the range of 0.17 MPa to 0.75 MPa before the collapse of the muscles, with a high value of 1.08 J·kg^{-1} with C of 2.9 and actuation stress of 0.75 kPa. The effective range for actuation load was enlarged with smaller C, at the cost of the smaller tensile strain as shown in Fig. 3(e). The tensile strain, normalized by the mandrel coil length after loading but before actuation, decreased with increasing actuation stress and decreasing spring index. A tensile strain of about 60% can be achieved if the spring index of 4.3 was selected.

3.3.2. Mechanism for tensile actuation of the mandrel-coiled bamboo muscles

To better understand the tensile actuation of the above muscles, the tensile strains should be recalculated and divided by the muscle length without actuation loading because it reflected the true actuation-induced length change without the interference of the loading-induced elongation, though the tensile strains normalized by the loaded length were meaningful in comparison with other types of artificial muscles. The actuation strain, which can be recognized as the actuation length change for muscles with the same coil length, gradually increased with rising humidity and spring index regardless of the type of mandrel coiling (Fig. 4(a)). The volume expansion was larger when more molecules were absorbed in higher humidity and the configurations with larger spring index helped improve tensile actuation strain. Besides the spring index, another geometrical parameter called the unit coil pitch (δ), which was defined as the distance between the axis of adjacent coils, was found to have an impact on the tensile strain of *ZZ* artificial muscles (Fig. 4(b)). Regardless of moisture flux, the contraction first increased to a peak value then decreased as δ increased from 0.75 mm to 2.5 mm. In the first stage, δ was too low for *ZZ* artificial muscles to have enough space for contraction. Thus, increasing δ resulted in higher contraction. In the second stage where enough space for actuation has been acquired, larger δ resulted in longer non-loaded length, thereby decreasing the tensile strain. The cycling results in Fig. 4(c) showed that the tensile stroke was stable for heterochiral and homochiral muscles during the investigated 20 actuation cycles, in accordance with the results shown in Fig. 3(b). Similarly, the tensile strain normalized by the non-loaded length in Fig. 4(d) declined with increasing applied stress or decreasing spring index, which was overall the same as that derived from Fig. 3(e). But the tensile strain here was higher than that in Fig. 3(e), especially when C was 3.6 or 4.3, in which the loading-induced elongation was large and had a significant impact on the calculated tensile strains.

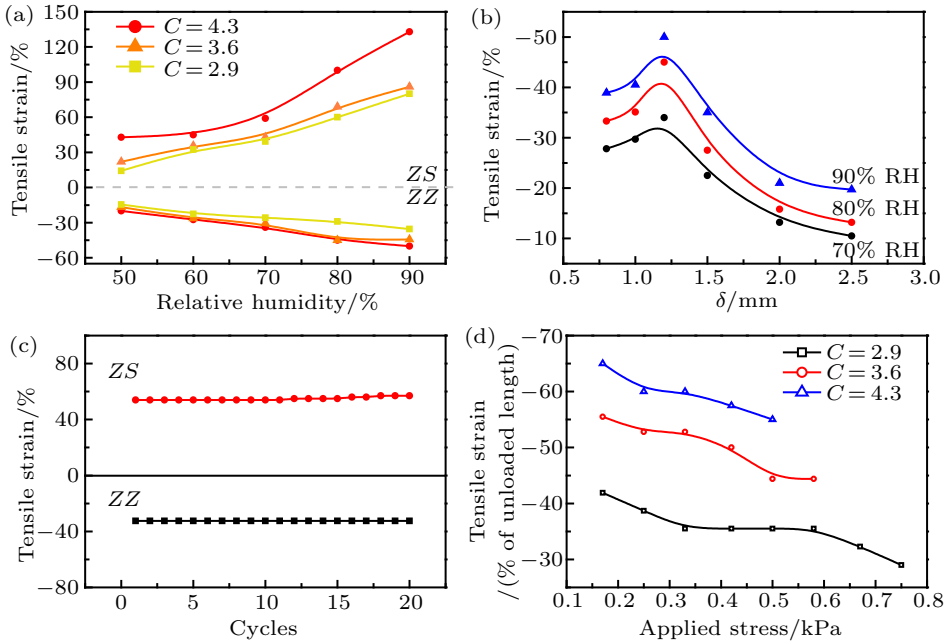


Fig. 4. Tensile actuation normalized by the non-loaded bamboo muscle length. (a) Tensile strains for muscles with different C that actuated in ambient humidity from 50%–90%. (b) Tensile strains as a function of coil pitch. (c) Cyclability of the tensile stroke for *ZS*- and *ZZ*-type muscles. (d) The non-loaded length normalized tensile strain as a function of applied stress for *ZZ* muscles with varied spring index. If not otherwise specified, the twist density was 900 turns·m^{-1}, the spring index was 4.3, the relative humidity was 70%, and the applied stress was 0.33 kPa for panels (a)–(d).

The tensile strain was affected by three categories of factors: the actuation stimulus, the applied load, and the geometry of the mandrel coiled muscles. The geometrical parameters of the mandrel coiled muscle included the inserted twist density, the unit coil pitch, and the spring index. With twist insertion and water molecule flux increasing to a possible high value and proper unit coil pitch selected, high actuation stress and low spring index benefit the mechanical work but limit the contraction strain for this *ZZ*-type mandrel coiled muscles. This kind of spring-shaped bamboo muscles was excellent in providing large contraction as compared with other types of artificial muscles.[24]

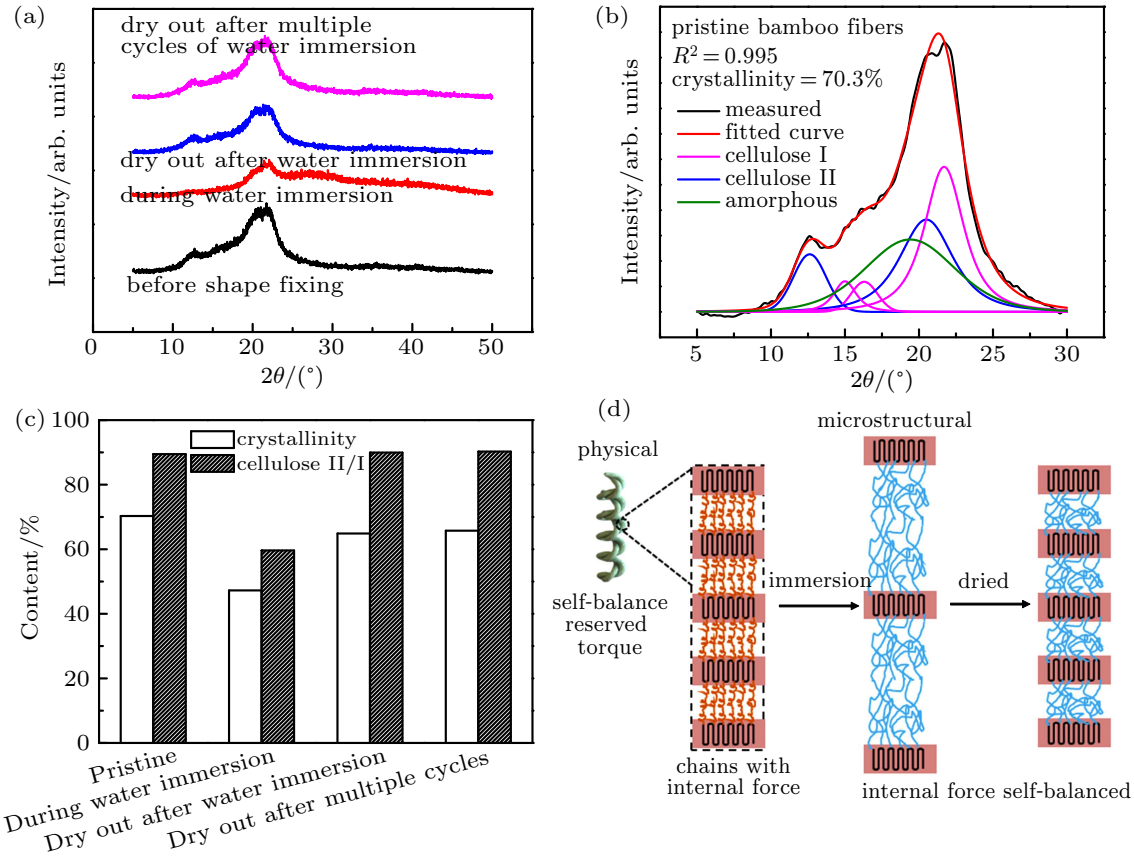


Fig. 5. The mechanism for shape fixing and actuation of mandrel coiled bamboo muscle. (a) X-ray diffraction curves for twisted muscles without treatments, followed by immersion in water, after shape fixing by drying out, and after multiple cycles of actuation. (b) The peak fitting profile for pristine bamboo fibers. (c) Crystallinity and the ratio of cellulose II to cellulose I for bamboo fibers with various treatment conditions. (d) Schematic illustration for the proposed mechanism of shape fixing and actuation for mandrel-coiled bamboo fibers.

As mentioned above, the shape of mandrel-coiled artificial muscles made by twisted and plied bamboo yarns can be fixed by water soaking and drying and actuated by water fog. XRD measurements were taken to elucidate the microstructural evolution during these processes (Fig. 5(a)). The pristine dry sample before shape fixing in water showed peaks at 2θ of 15.0°, 16.3°, and 22.7°, referring to the cellulose I and peaks at 2θ of 12.2° and 20.1°, corresponding to the cellulose II.[25] The peak devolution results were obtained with steps stated in Subsection 2.4 (Fig. 5(b)) and the crystallinity was calculated as 70.3%, with the ratio of cellulose II to cellulose I as 0.895 (Fig. 5(c)). Then the pristine sample was immersed in water for 10 min and then immediately tested. The content of the cellulose II phase decreased and a new and wide peak at 2θ of 28.2° was observed, showing that the water molecules can gradually enter between the cellulose chains and make the crystal phases, especially the cellulose II phase to be more amorphous. The peak fitting results further proved that by the decreasing value of crystallinity of 47.2% and the ratio of cellulose II to cellulose I as 0.596. In this process, some internal stress by twist insertion was released, but most internal stress was retained because of the self-balanced structures of the plied yarns. After water immersion followed by evaporation, the crystallinity returned to 64.9%, and the ratio of cellulose II to cellulose I increased to 0.900, showing that the cellulose II phase regenerated to form a new level of physical crosslink to fix the shape. Note that the crystallinity may decrease a little bit but after multiple cycles of immersion and evaporation, the crystallinity (65.7%) and the ratio of cellulose II to cellulose I (0.903) kept stable, showing that the

bamboo fibers could be a potential candidate for shape memory behavior. The mechanism was summarized and illustrated in Fig. 5(d). The twist insertion of bamboo yarns introduced torques into the actuator, with some of them balanced by bamboo yarn plying. After mandrel coiling, the internal stress was still not balanced until the water immersion process took place. The decreased crystallinity contributed to the release of segments with internal force. After drying, the crystals including cellulose I and II could be regenerated and fix the shape. Because the exposure time to water fog during actuation was short (< 10 s), the cellulose crystals can not be destroyed permanently as with the case of water immersion and the main actuation force was from the volume expansion of the yarns by absorbing water molecules. Thus, even after multiple cycles of actuation, the contents of cellulose I and cellulose II phases were negligibly changed, in accordance with the good cyclability of actuation.

3.3.3. Demonstration of mandrel-coiled bamboo muscles for smart textiles

Because of the high sensitivity and large actuation strokes of the bamboo actuators, the mandrel coiled bamboo muscles were here used for the demonstration of smart textiles. As shown in Fig. 6 and Movie S1, a skirt was tethered on the mandrel coiled bamboo muscles. With ambient humidity increased to about 70%, the length of the skirts decreased to improve the comfortability of users due to the contraction motion and the work capacity provided by the *ZZ*-type bamboo muscles (Figs. 6(a) and 6(b)). However, after the ambient humidity decreased to normal, the length of the skirts could return to ensure air permeability (Fig. 6(c)). Thanks to the self-balanced structure and the water immersion treatment, the bamboo actuators can work without additional tethering, which facilitated their integration into smart textiles.

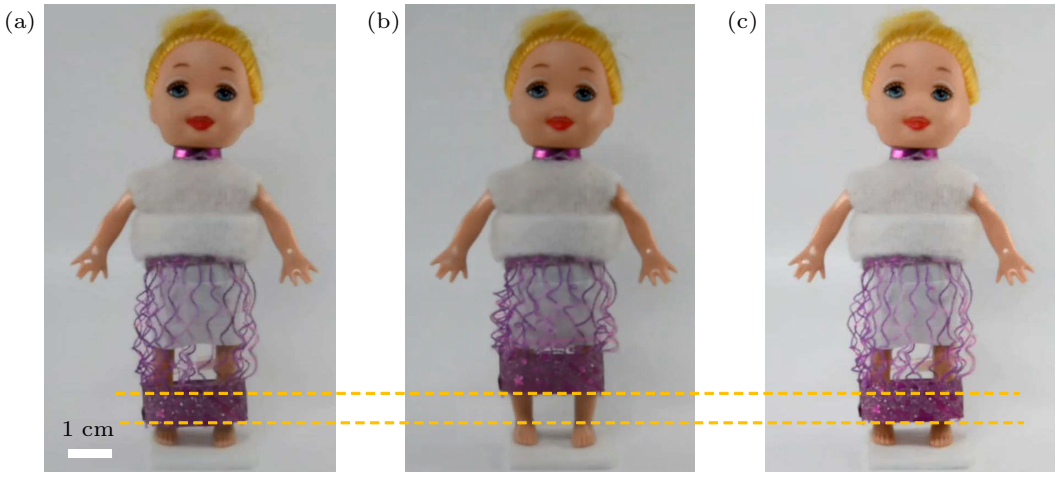


Fig. 6. Demonstration of the *ZZ* mandrel coiled bamboo fibers for intelligent smart skirts under moisture activation, with photos (a) before actuation, (b) during actuation, and (c) after actuation.

4. Conclusion and perspectives

In short, the porous bamboo yarns were folded in the midpoint to fabricate self-balanced torsional actuators with a maximum torsional stroke of $64.4°\cdot mm^{-1}$ in 4.2 s under 90% relative humidity. Subsequent mandrel coiling and water immersion shape fixing produced tensile artificial muscles, which showed the maximum contraction of 50% and work capacity of $1.08\ J\cdot kg^{-1}$. The effect of geometrical parameters on the tensile elongation was studied based on the volume expansion mechanism by water molecule absorption. The hierarchical porous structure of bamboo yarns together with the hydrophilicity of bamboo yarns was the origin of high sensitivity and fast actuation upon water fog. By immersing the bamboo yarns into water for a relatively long period, the content of the crystal phase was diminished, which could be regenerated after drying. The above microstructural evolution was responsible for shape fixing and good cyclability of tensile actuation. By detailed structural, physical, and chemical research of the actuation performances, this work may put insights on the application of bamboo yarns for smart textiles.

References

[1] Jin H, Matsuhisa N, Lee S, Abbas M, Yokota T and Someya T 2017 *Adv. Mater.* **29** 1605848
[2] Zhang X, Chen X, Bai T, You X Y, Zhao X, Liu X Y and Ye M D 2020 *Acta Phys. Sin.* **69** 178201 (in Chinese)
[3] Gong W, Hou C, Guo Y, Zhou J, Mu J, Li Y, Zhang Q and Wang H 2017 *Nano Energy* **39** 673
[4] Park M, Im J, Shin M, Min Y, Park J, Cho H, Park S, Shim M B, Jeon S, Chung D Y, Bae J, Park J, Jeong U and Kim K 2012 *Nat. Nanotechnol.* **7** 803
[5] Wang Q W, Zhang H B, Liu J, Zhao S, Xie X, Liu L, Yang R, Koratkar N and Yu Z Z 2019 *Adv. Funct. Mater.* **29** 1806819
[6] Morin S A, Shepherd R F, Kwok S W, Stokes A A, Nemiroski A and Whitesides G M 2012 *Science* **337** 828
[7] Li Y, Zhang Z, Li X, Zhang J, Lou H, Shi X, Cheng X and Peng H 2017 *J. Mater. Chem. C* **5** 41

[8] Lou M, Abdalla I, Zhu M, Wei X, Yu J, Li Z and Ding B 2020 *ACS Appl. Mater. Interfaces* **12** 19965
[9] Wang Y, Liang X, Zhu H, Xin J H, Zhang Q and Zhu S 2020 *Adv. Funct. Mater.* **30** 1907851
[10] Uzun S, Seyedin S, Stoltzfus A L, Levitt A S, Alhabeb M, Anayee M, Strobel C J, Razal J M, Dion G and Gogotsi Y 2019 *Adv. Funct. Mater.* **29** 1905015
[11] Tao Y, Liu Q, Chen J, Wang B, Wang Y, Liu K, Li M, Jiang H, Lu Z and Wang D 2016 *Environ. Sci. Technol.* **50** 7889
[12] Puls J, Wilson S A and Hölter D 2011 *J. Polym. Environ.* **19** 152
[13] Li S, Liu J, Wen H, Liu X and Guo W 2020 *Acta Phys. Sin.* **69** 178703 (in Chinese)
[14] Pan L, Wang F, Cheng Y, Leow W R, Zhang Y W, Wang M, Cai P, Ji B, Li D and Chen X 2020 *Nat. Commun.* **11** 1332
[15] Li Y Y, Leng X Q, Sun J K, Zhou X, Wu W, Chen H and Liu Z F 2020 *Chin. Phys. B* **29** 048103
[16] Le Duigou A and Castro M 2015 *Ind. Crop. Prod.* **71** 1
[17] Wang Y, Wang G, Cheng H, Tian G, Liu Z, Feng X Q, Zhou X, Han X and Gao X 2010 *Text. Res. J.* **80** 334
[18] Zhao Y, Fang F, Xiao H M, Feng Q P, Xiong L Y and Fu S Y 2015 *Chem. Eng. J.* **270** 528
[19] Afrin T, Tsuzuki T, Kanwar R K and Wang X 2012 *J. Text. I.* **103** 844
[20] Cheng H, Hu Y, Zhao F, Dong Z, Wang Y, Chen N, Zhang Z and Qu L 2014 *Adv. Mater.* **26** 2909
[21] Chen P, Xu Y, He S, Sun X, Pan S, Deng J, Chen D and Peng H 2015 *Nat. Nanotechnol.* **10** 1077
[22] Jia T J, Wang Y, Dou Y Y, Li Y W, de Andrade M J, Wang R, Fang S L, Li J J, Yu Z, Qiao R, Liu Z J, Cheng Y, Su Y W, Minary-Jolandan M, Baughman R H, Qian D and Liu Z F 2019 *Adv. Funct. Mater.* **29** 1808241
[23] Haines C S, Lima M D, Li N, Spinks G M, Foroughi J, Madden J D W, Kim S H, Fang S, De Andrade M J, Göktepe F, Göktepe Ö, Mirvakili S M, Naficy S, Lepró X, Oh J, Kozlov M E, Kim S J, Xu X, Swedlove B J, Wallace G G and Baughman R H 2014 *Science* **343** 868
[24] Mirvakili S M and Hunter I W 2018 *Adv. Mater.* **30** 1704407
[25] Liu Y P and Hu H 2008 *Fiber Polym.* **9** 735